Proceedings of Global Power and Propulsion Society
ISSN-Nr: 2504-4400
GPPS Hong Kong 2023
October 17-19, 2023
www.gpps.global

GPPS-TC-2023-105

Numerical simulation of inlet total pressure distortion on a two-stage high-speed axial fan

Hongliang Zhao
[1] School of Energy Power and Mechanical Engineering, North China Electric Power University
zhaohl333@163.com
Beijing, 102206, China

Wenqiang Zhang
[4] School of Mechatronical Engineering, Beijing Institute of Technology
wenqiangzhang@bit.edu.cn
Beijing 100081, China

Jiahui Qiu
[2]Institute of Engineering Thermophysics, Chinese Academy of Sciences, [3]University of Chinese Academy of Sciences
qiujiahui@iet.cn
Beijing, 100190, China

Min Zhang
[2]Institute of Engineering Thermophysics, Chinese Academy of Sciences, [3]University of Chinese Academy of Sciences
zhangmin@iet.cn
Beijing, 100190, China

Juan Du
[2]Institute of Engineering Thermophysics, Chinese Academy of Sciences, [3]University of Chinese Academy of Sciences
dujuan@iet.cn
Beijing, 100190, China

Chaoqun Nie
[2]Institute of Engineering Thermophysics, Chinese Academy of Sciences, [3]University of Chinese Academy of Sciences
ncq@iet.cn
Beijing, 100190, China

ABSTRACT

Inlet total pressure distortion is a critical factor affecting aero engines' performance and stability. Steady calculations are conducted for a two-stage fan under uniform inlet conditions. Full annular unsteady simulations of an inserted baffle distortion generator coupled with a two-stage fan are conducted under distorted inlet conditions. Numerical calculation results show that the baffle distortion generator mainly contributes to the total pressure distortion in the fan inlet surface. The total pressure distortion induces the total temperature distortion. The transfer and distribution of the two-stage fan's total pressure and temperature distortions are calculated and analyzed. After the airflow goes through the fan, the intensity of total pressure distortion is weakened, the intensity of total temperature distortion is enhanced, and the total temperature and static entropy at the blade tip region after turning out of the corresponding distortion baffle are more significant. The flow field after the baffle shows a symmetrical double vortex structure, which causes the positive and negative pre-swirl distribution of airflow angle and lower axial velocity.

Keywords: axial flow fan, total pressure distortion, baffle, total temperature distortion, unsteady simulation

INTRODUCTION

The inlet total pressure distortion can cause fan or compressor destabilization, limiting engine performance and being one of the most significant factors in aero-engine stability(Biesiadny et al., 1986, Reid, 1969, Williams, 1987, Longley and Greitzer, 1992). Researchers have conducted total pressure distortion tests with various types of distortion generators. The Americans have manufactured different types of distortion generators and installed them in the engine intakes to simulate different types and intensities of total pressure distortion(Bobbala, 1979, Graber Jr and Braithwaite, 1974, Cramer, 2002). Based on numerous inlet distortion tests, The Society of Automotive Engineers (SAE) has summarized and published an aerospace-recommended practice document on definitions of stability margin and total pressure distortion descriptors for gas turbine engines, ARP-1420.

Most domestic researchers have learned from the Russian adjustable insert-type total pressure distortion generator(Ogorodnikov, 1993) to simulate the effect of total pressure distortion on the compressor. Li et al.(Li et al., 2020) have conducted an experimental study on the radial distortion of the inlet duct of a three-stage axial flow compressor. The test results show that the radial distortion mainly deteriorates the flow in the first stage, including the tip leakage flow and aerodynamic parameters, and the flow deterioration caused by the inlet distortion is recovered in the third stage of the

compressor. Gunn et al.(Gunn et al., 2013) have experimentally measured the effect of a 60° circumferential range total pressure distortion on the low-speed fan stage. The analysis reveals that the inlet distortion causes the incidence angle of the rotor leading edge to deviate from the design value, which leads to an increase in rotor losses, and the flow separation caused by the whirl angle distortion at the rotor exit increases the losses of the stator row. Xia et al.(Aiguo et al., 2018) developed a controlled-variable double-baffle distortion generator in a horizontally symmetrical moving form and performed total pressure distortion tests. The results show that the distortion generator can simulate steady-state and transient distortions. There is a critical insertion depth beyond which the symmetric baffles will generate an asymmetric flow field. Moreover, the engine's instability differs from that under a single baffle. Li et al.(Li et al., 2009) conducted an experimental study on the total inlet pressure distortion with four different types of baffles on a two-stage low-speed axial flow compressor. The results indicate that the effect of the total inlet pressure distortion on the compressor stability and performance is significant. The blocking area significantly affects the performance, while the characteristic angle formed by the baffles has no pronounced effect on the performance.

This paper introduces the two-stage fan study object and the main steady and unsteady calculation settings. Then, the fan characteristics and internal flow fields of typical operating conditions are compared between the steady calculation results and experimental data under uniform inflow. Subsequently, the total pressure and induced total temperature distortion transfer characteristics as well as the internal flow field evolution are analyzed based on the unsteady calculation results of the two fan-coupled inserted baffles distortion generator. Finally, the main conclusions are obtained.

METHODOLOGY

The two-stage high-speed axial fan test stand is shown in Figure 1. A synchronous motor with 15000kW power drives the fan. The critical parameters of the fan are shown in Table 1, with a design speed of 13200 rpm and a tip clearance of 0.2 mm. The computational domain of the full-annulus of the two-stage fan coupled by the inserted baffle distortion generator under the total pressure distortion inlet condition remains consistent with the experiment, as shown in Figure 2, where the axial distance of the baffle from the AIP (aerodynamic interface plane) plane is three times the rotor diameter.

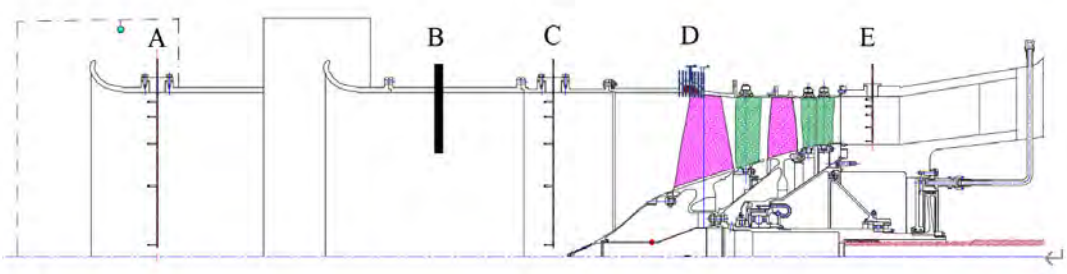

Figure 1 Schematic diagram of the test rig

Table 1 Key parameters of the two-stage fan

Parameter	Value
Design speed	13200 rpm
Rotor tip clearance	0.2 mm
Rotor corner radius	5 mm
Number of rotor blades in stage 1	19
Number of stator blades in stage 1	42
Number of rotor blades in stage 2	29
Number of stator blades in stage 2	54

The grid of the computational domain is generated by NUMECA/AutoGrid5. The minimum orthogonal angle of the model is 22.8°, the maximum aspect ratio is 1503, and the maximum expansion ratio reaches 2.02, which satisfies the mesh quality requirements. It is ensured that y+<3. Therefore, the number of grids accounted for on a single passage of the two-stage fan is about 3.5 million, and the total number of grids reaches 113 million for the entire annulus. The software ANSYS CFX is applied to solve the Reynolds-averaged Navier-Stokes (RANS/URANS) equation. The turbulence model is the *k-ω*model, the interface type between the rotor and the stator mixing plane for steady simulation, and the transient rotor-

stator for unsteady simulation. In addition, unsteady calculations use the results of steady calculations as the initial fields to accelerate the convergence.

Figure 2 Schematic diagram of the computational domain

RESULTS AND DISCUSSION

Uniform Inflow

The comparison between the simulated and experimental values of the characteristics map of the two stages fan at different speeds of 0.8n and 1.0n under uniform incoming flow is shown in Figure 3. The overall fan pressure ratio characteristics match very well at different speeds; the simulated value of the isentropic efficiency at 0.8n is lower than the experimental value, which may be related to the local temperature variation.

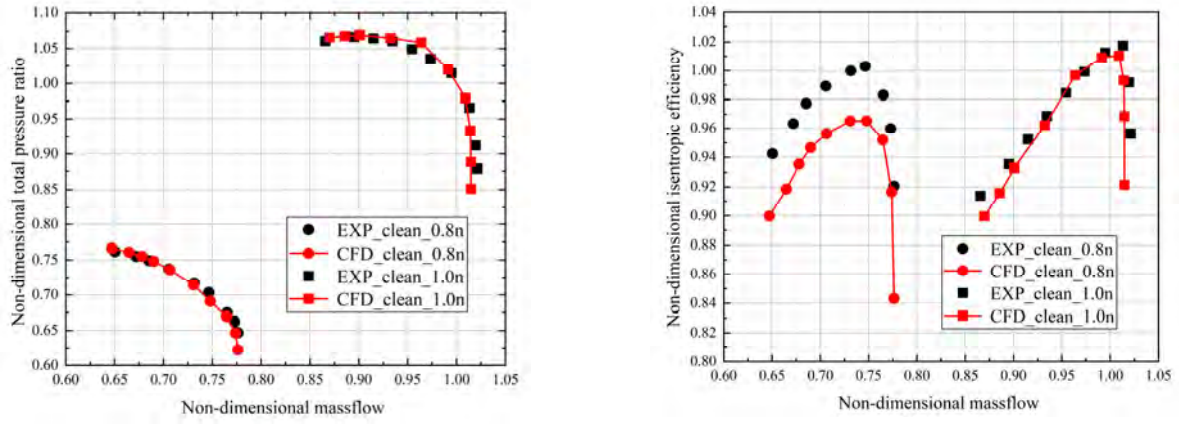

(a) Total pressure ratio (b) Isentropic efficiency

Figure 3 Comparison of numerical simulation and experimental data under uniform flow

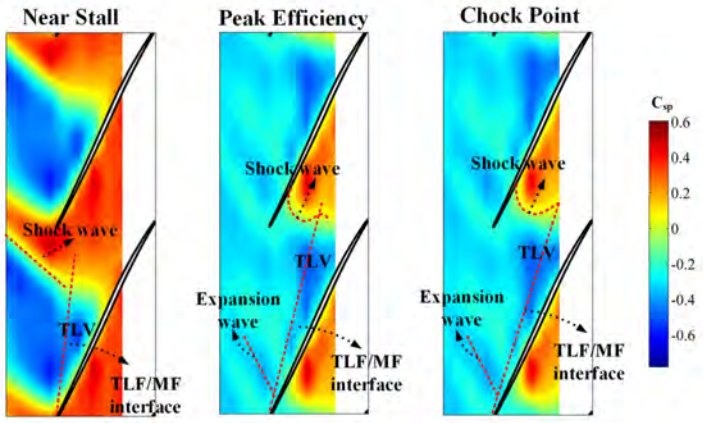

(a) Experimental measurement results

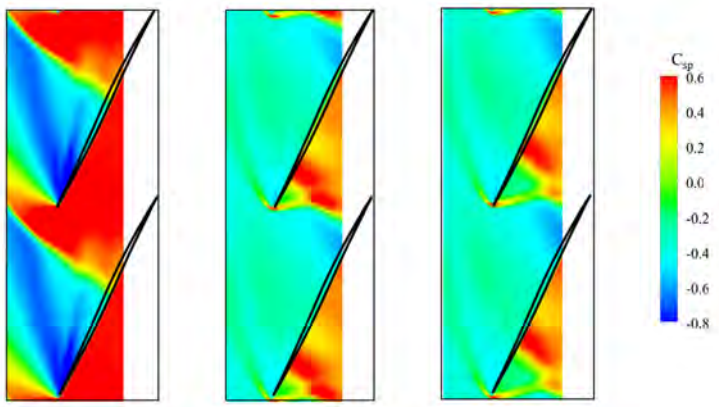

(b) Numerical simulation results

Figure 4 Comparison of the internal flow field for three typical operating conditions

Furthermore, the static pressure contour at the blade tip of the first rotor is compared and analyzed for three typical operating conditions at 100% speed (near stall point, peak efficiency point, and chock point, respectively). Figure 4(a) shows the experimental results, while Figure 4(b) shows the numerical simulation value at 0.999 span. It can be seen that the numerical simulation accurately captures the intensity and position of the tip leakage flow as well as the shock wave moving forward from the passage to the leading edge of the blade until spilling out.

Distortion Inflow

Figure 5 shows the total pressure ratio and isentropic efficiency obtained from the numerical simulations compared with the experimental data under the total pressure distortion flow. The black square and curve represent the experimental and simulated values under uniform inlet conditions. The red dot and red curve represent the experimental and simulated values under total pressure distortion inlet conditions, respectively, which are a good match. By taking the efficiency of the design point of the two-stage fan as the standard, the efficiency of each operating point is divided by the design point efficiency to obtain the non-dimensional efficiency. It occurs that the non-dimensional efficiency at some points is greater than 1.0 since the design point is not the peak efficiency point. Then, the peak efficiency point analysis for the unsteady calculation under the total pressure distortion condition is performed.

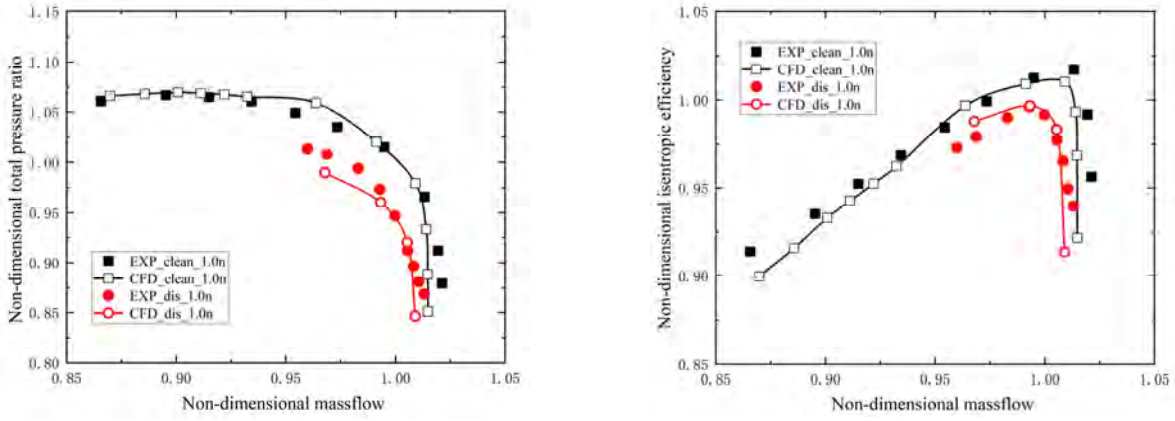

(a) Total pressure ratio (b) Isentropic efficiency

Figure 5 Comparison of numerical simulation and experimental data under distortion flow

Figure 6 shows the total pressure transmission from the distortion baffles to the inlet surface of the fan's first-stage rotor. Figure 7 presents the three-dimensional streamlines behind the distortion baffle. As the figure shows, a prominent low total pressure region is formed behind the distortion baffle. The closer the fan inlet surface is, the lower the total pressure inhomogeneity is due to the mixing of high and low-pressure regions. In addition, a symmetrical twin swirl structure is formed due to the effect of the distortion baffle.

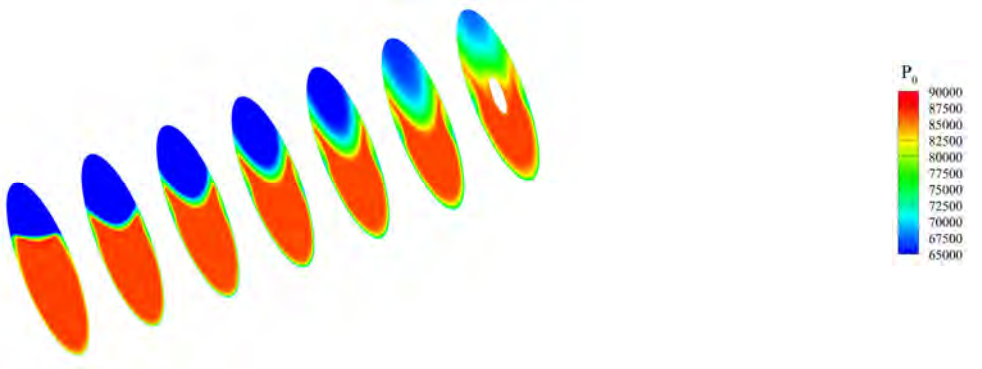

Figure 6 Total pressure distribution in different axial positions behind the baffle

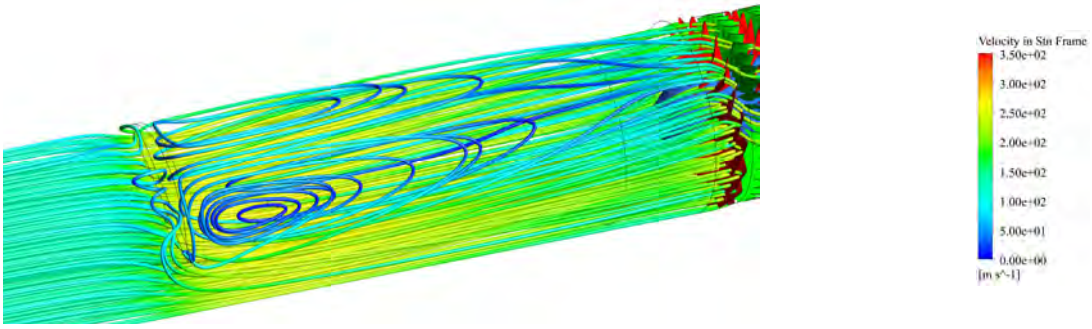

Figure 7 Three-dimensional streamline distribution behind the baffle

Characteristics of Distortion Transfer

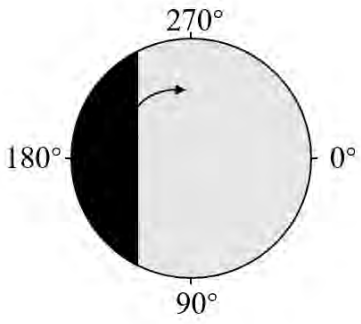

Figure 8 Schematic diagram of the baffle and angle definition

Figure 8 shows a schematic diagram of the depth of the baffle and the definition of the circumferential angle. Figure 9 shows the circumferential distribution of the total pressure and temperature at the first-stage inlet surface, the first-stage outlet surface (second-stage inlet surface), and the second-stage outlet surface at three different blade spans for 1.0n speed under the total pressure distortion inlet condition. As can be seen from the figure, at 0.1 spans, the intensity of the low pressure on the first stage inlet surface is small, and the total temperature is almost unchanged; through the first stage of the fan, the range of the low total pressure region is expanded, and the intensity is enhanced, the range of total temperature distortion is enlarged, and the total temperature value of the turning out distortion region is more significant; at the exit surface of the second stage of the fan, the range and intensity of the total pressure distortion are reduced, while the total temperature distortion is still increased.

As the position of the blade spans increases, at 0.5 and 0.9 spans, the range and intensity of the low total pressure at the first stage inlet surface are more prominent, and a slight fluctuation of about 2K in total temperature. At the first stage outlet surface, the total pressure and the total temperature trends decrease first and then increase, corresponding to the position of the distortion baffle; the total pressure and the total temperature have the lowest values. On the second stage exit surface, at 0.5 spans, the total pressure exhibits a low total pressure range along the circumference; after turning out of the corresponding position of the distortion baffle, the total temperature displays a high total temperature peak. At 0.9 span, the intensity of total pressure distortion decreases dramatically. It is almost circumferentially uniform, which is due to the work done by the fan to input energy to the low-pressure region. Then the total temperature circumferential distribution

has a more obvious peak and two valleys, indicating that the total temperature distortion intensity is enhanced, which is related to the environmental temperature of the airflow, the fan rotation speed and the ability of the fan to fight temperature distortion.

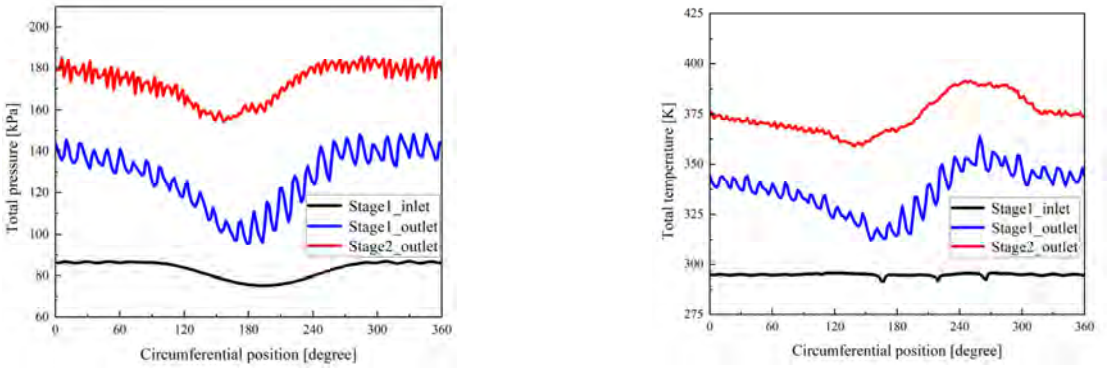

(a) 0.1span

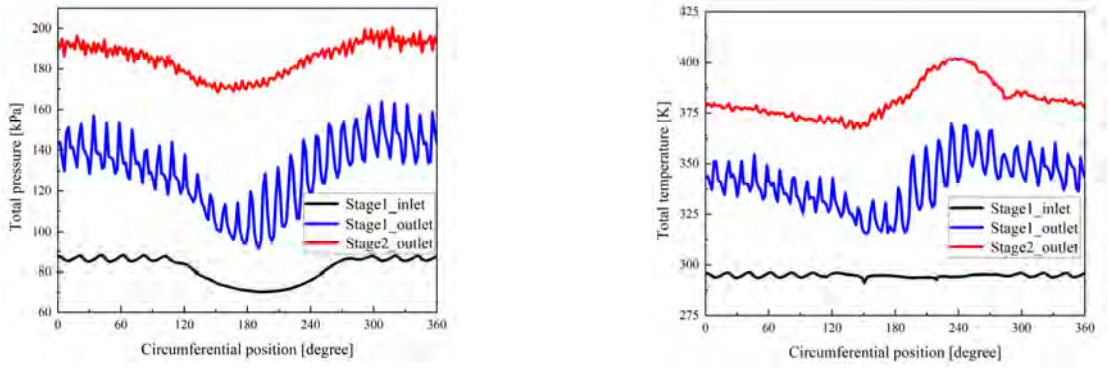

(b) 0.5span

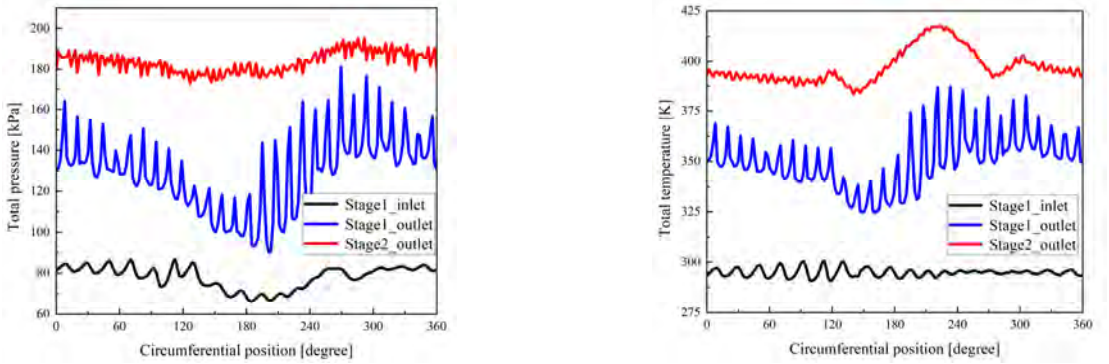

(c) 0.9span

Figure 9 Circumferential distribution of total pressure and temperature at the inlet and outlet surfaces of different stages

Figure 10 shows the contour of axial velocity distribution at the fan's inlet AIP (C-C) and outlet AIP (E-E). At the C-C AIP, a large area of lower axial velocity is at the corresponding position behind the distortion baffle. Two small symmetrical areas of lower axial velocity are at the junction of the corresponding positions of the distortion and non-distortion regions. At the E-E AIP, the axial velocity is lower at the position corresponding to the rotation into the distortion baffle near the hub.

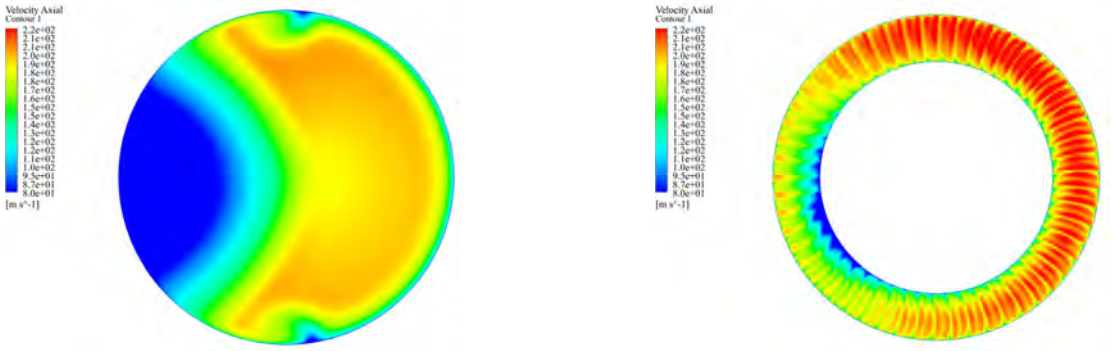

(a) AIP(C-C) (b) AIP(E-E)

Figure 10 Contour of axial velocity at AIPs

Figure 11 shows the contour of static entropy distribution at the fan's inlet AIP (C-C) and outlet AIP (E-E). At the C-C AIP, the static entropy value is more prominent at the corresponding position after the distortion baffle. After flowing through the fan, At the E-E AIP, the static entropy value of the corresponding position of the rotation out distortion baffle near the blade tip is more considerable, indicating that the flow losses are higher here, which is related to the local total temperature intensity.

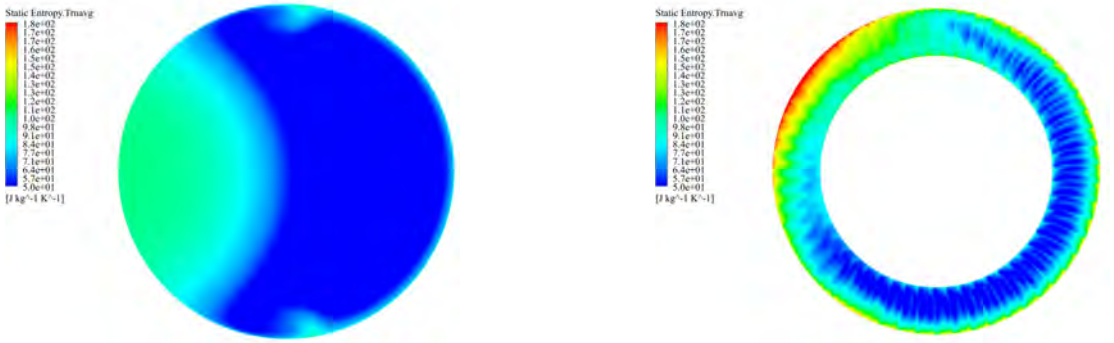

(a) AIP(C-C) (b) AIP(E-E)

Figure 11 Contour of static entropy at AIPs

Figure 12(a)、(b) shows the contour of flow angle distribution at the C-C AIP and the inlet surface of the first stage rotor, respectively. As can be seen from the figure12, the flow angle on the C-C AIP surface shows a symmetrical distribution of positive and negative pre-swirl, and the positive pre-swirl intensity at the corresponding position of the turn-in distortion baffle is greater than the negative pre-swirl at the turn-out position. As the first stage rotor inlet surface approaches, the circumferential and radial distribution of pre-swirl becomes more non-uniform, and the intensity of the negative pre-swirl becomes larger at the downstream position where the rotor turns out of the distortion region. It is inferred that the flow at the downstream position is susceptible to deterioration.

(a) AIP(C-C) (b) At the first stage rotor inlet surface

Figure 12 Contour of flow angle distribution at different axial positions

Finally a comparison of the axial velocity at different span in the R1 domain at near stall point is shown in figure 13. From figure 13(a), it can be seen that the change of axial velocity at different circumferential positions in the R1 domain at 0.10 span is not significant; figure 13(b) shows a decrease in the axial velocity at the leading edge (LE) of R1 in the distortion region at 0.50 span; figure 13(c) shows contour of axial velocity at 0.99 span, which shows a significant decrease in axial velocity for the downstream blade passage and at the trailing edge (TE) of the blade suction surface. This further

confirms that the flow is susceptible to instability when the rotor blade turns from the distortion region to the downstream, and it starts from the blade tip region.

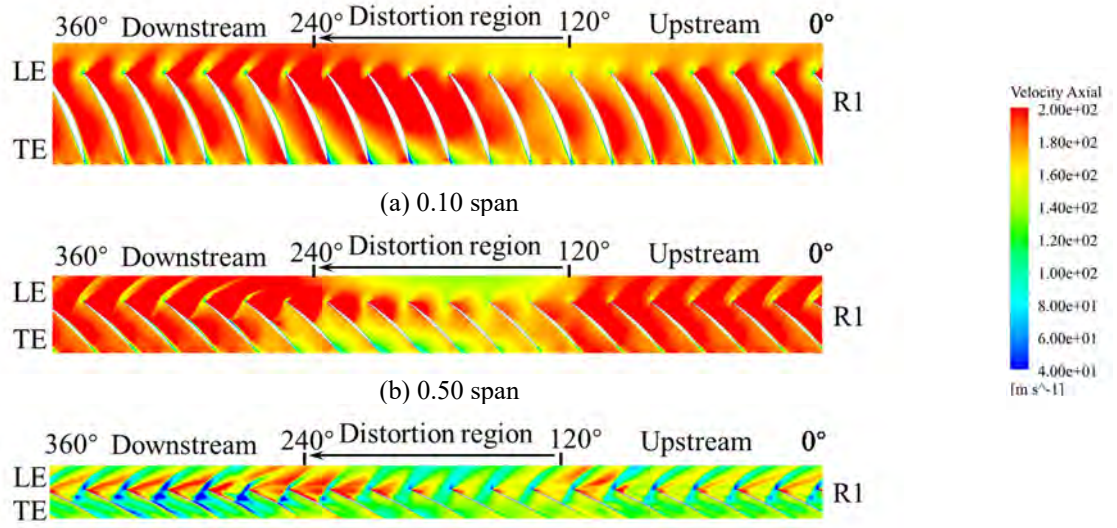

(a) 0.10 span

(b) 0.50 span

(c) 0.99 span

Figure 13 Contour of axial velocity at different span at near stall point

CONCLUSIONS

In this paper, a two-stage high-speed axial fan is computed with a single passage steady under uniform inflow and a full annular unsteady calculation for a fan coupled with an inserted baffle distortion generator. The main conclusions are as follows:

(1) The simulation can accurately capture the flow characteristics of the fan by comparing the overall fan characteristics and the internal flow field of different typical operating conditions with the experimental results under uniform inflow conditions.

(2) The inserted baffle distortion generator mainly causes total pressure distortion, which reduces the pressure ratio and isentropic efficiency of the fan. When the airflow through the fan, the total pressure distortion triggers the total temperature distortion, and the circumferential range and intensity of the total pressure distortion decrease. Meanwhile, the circumferential range and intensity of the total temperature distortion increase.

(3) The results of the unsteady calculation of the full annular of the two-stage fan coupled with the distortion generator are in good agreement with the experimental data, and the unsteady calculation can clearly describe the distribution of various parameters in each section in both circumferential and radial directions as well as the internal flow field disturbances. The total pressure and axial velocity after the distortion baffle is lower, and there is an apparent symmetry of the double vortex phenomenon, causing the rotor blade leading edge to have positive and negative pre-swirl distribution, and the intensity of the negative pre-swirl is larger at the downstream of the distortion region. The comparative analysis of axial velocity at different span at the near stall point further indicates that flow instability is susceptible to occur at the downstream of the distortion region.

ACKNOWLEDGMENTS

The authors are grateful for the support of the support of the National Science and Technology Major Project (2017-II-0004-0017).

References

AIGUO, X., HUANG, X., WEI, T. & MING, Z. J. C. J. O. A. 2018. Experimental study of a controlled variable double-baffle distortion generator engine test rig. 31**,** 1880-1893.

BIESIADNY, T. J., BRAITHWAITE, W. M., SOEDER, R. H. & ABDELWAHAB, M. Summary of investigations of engine response to distorted inlet conditions. Meeting of the Propulsion and Energetics Panel, 1986.

BOBBALA, G. 1979. Effect of steady-state pressu\re distortion on stall margin of a J85-21 turbine engine. NASA-TM-79123 E-9958 NASA Lewis research center.

CRAMER, K. B. 2002. *Design of a total pressure distortion generator for aircraft engine testing.* Virginia Tech.

GRABER JR, E. & BRAITHWAITE, W. M. Summary of recent investigations of inlet flow distortion effect on engine stability. Aerospace Sci. Meeting, 1974.
GUNN, E. J., TOOZE, S. E., HALL, C. A. & COLIN, Y. J. J. O. T. 2013. An experimental study of loss sources in a fan operating with continuous inlet stagnation pressure distortion. 135**,** 051002.
LI, J., DU, J., LIU, Y., ZHANG, H., NIE, C. J. A. S. & TECHNOLOGY 2020. Effect of inlet radial distortion on aerodynamic stability in a multi-stage axial flow compressor. 105**,** 105886.
LI, L., HU, J., WANG, Z. & TU, B. J. J. O. A. P. 2009. Experimental study of inlet total-pressure distortion on four kinds of flat baffles. 24**,** 925-930.
LONGLEY, J. & GREITZER, E. Inlet distortion effects in aircraft propulsion system integration. Steady and transient performance prediction of gas turbine engines, 1992. Advisory Group for Aerospace Research and Development (AGARD).
OGORODNIKOV, D. Real-time simulation of maneuverable aircraft flight conditions on altitude test cell. 29th Joint Propulsion Conference and Exhibit, 1993. 1845.
REID, C. 1969. *The response of axial flow compressors to intake flow distortion*, American society of mechanical engineers.
WILLIAMS, D. 1987. Review of current knowledge on engine response to distorted inflow conditions.